Tellus (2007), 59A, 279–291
Printed in Singapore. All rights reserved

TELLUS

Parametrization of orographic effects on surface radiation in HIRLAM

By A. V. SENKOVA[1], L. RONTU[2,*] and H. SAVIJÄRVI[3], [1]*Russian State Hydrometeorological University, St.Petersburg, Russia;* [2]*Finnish Meteorological Institute, Helsinki, Finland;* [3]*University of Helsinki, Helsinki, Finland*

(Manuscript received 15 September 2006; in final form 19 February 2007)

ABSTRACT

A parametrization scheme for orographic effects on surface radiation was introduced in the High Resolution Limited Area Model. One-kilometre resolution digital elevation data were used to derive the needed orographic parameters. The scheme is applicable within a model setup of any resolution, but is shown to significantly affect the local near-surface temperatures only when the horizontal resolution is less than a few kilometres. Then, typical maximum local differences due to the new parametrizations are 50–100 W m^{-2} in the net radiation fluxes and 1°–3° in the screen-level temperature. Interactions between clouds and radiation were detected both in the single-column and three-dimensional sensitivity experiments.

1. Introduction

The purpose of a radiation parametrization scheme in a numerical weather prediction (NWP) model is to calculate the grid-scale air temperature change due to the solar and terrestrial radiation. In addition, the scheme provides components of the surface radiation balance, that is, the upwelling and downwelling radiation fluxes at the surface. The radiation scheme of the High Resolution Limited Area Model (HIRLAM), based on Savijärvi (1990) and and Wyser et al. (1999), divides the spectrum of radiation to two spectral bands only, handling long- and short-wave parts separately. More detailed schemes, applied in general circulation models, use several bands for both short- and long-wave calculations. Assumptions concerning cloud–radiation interactions vary in the models, depending on available information of aerosol, cloud and precipitation particles.

For calculation of the surface radiation fluxes, the grid-averaged short-wave albedo and long-wave emissivity, as well as the surface (skin) temperature, are necessary. These properties of the underlying surface may be provided by the surface description (physiography), surface data assimilation and parametrization schemes of the model. In HIRLAM, both constant and temporally evolving properties of the surface subtypes (water, snow and ice, low vegetation, forest, urban, etc.) influence the values of albedo and emissivity. In addition to the averaged albedo and emissivity, only the grid-scale mean surface elevation in the terrain-following, pressure-based hybrid coordinate of HIRLAM, is known to its present radiation scheme. From the point of view of the atmospheric radiation parametrizations, each gridsquare is therefore assumed flat and effectively homogeneous.

On the other hand, the grid-average downwelling short- and long-wave radiative fluxes at the surface, provided by the radiation scheme, may be used as input for detailed calculation of surface energy balance over different surfaces, for example, within forest or urban canopy or at a road surface. Typically, such localized applications would require additional information about the surface with high horizontal and vertical resolution, well beyond even the present-day kilometre-scale non-hydrostatic NWP models. In HIRLAM, the surface energy balance for each surface subtype of a gridsquare is handled by a tiled surface parametrization scheme (Rodriguez et al., 2003). Specific albedo, emissivity and surface temperature values for each surface type are used to calculate the respective upwelling fluxes.

In the intermediate scale, correct handling of the orographic effects on surface radiation becomes increasingly important, when the resolution of NWP models is increased to produce realistic local weather forecasts. The surface radiation balance in a location at, or in the vicinity of mountains, is influenced by the local surface elevation, local horizon and by steepness and direction of surrounding slopes. Significant short- and long-wave radiation (SWR and LWR) effects on the surface temperature over complex terrain have been reported by Dubayah & van Katwijk (1992), Matzinger et al. (2003), Whiteman et al.

*Corresponding author.
e-mail: laura.rontu@fmi.fi
DOI: 10.1111/j.1600-0870.2007.00235.x

(1989a,b), Nunes et al. (2000) and Oliphant et al. (2003), among others.

In principle, accounting for the orographic effects on radiation is a simple geometric exercise. The basic theory is well known since Kondratyev et al. (1978). However, the operational NWP environment poses specific constraints for parametrization of this four-dimensional problem, where time-dependency is non-linearly combined with three-dimensional, (non-local) orography features. Müller & Scherer (2004, 2005) were the first to publish a scheme which used high-resolution subgrid-scale orography information for the calculation of radiation effects over complex terrain. The authors formulated a unified method to parametrize the SWR effects due to different slope angles and directions, relief shadows (for SWR) and restricted sky view (both for SWR and LWR). Their results indicated, that introduction of the parametrizations into the Non-hydrostatic Mesoscale Model (NMM) improved the 2-m temperature forecasts over the Alps. Liang et al. (2006) tested an application of Müller-Scherer scheme in the climate version of Weather Research and Forecast model (CWRF). Only minor impact was seen in their experiments, evidently because of the coarse model resolution.

We suggest a scheme of orographic radiation parametrizations for HIRLAM. The parametrizations are based a few main principles and assumptions. First, the scheme should utilize the most detailed (subgrid-scale) orography information available. In the parametrization, radiation fluxes should be averaged, not the orography. Second, the orographic effects on radiation are estimated by modifying the downwelling SWR and LWR fluxes at the surface level, provided by the basic radiation scheme. Third, the scheme is formulated in the framework of the physical parametrizations of the present day NWP models, where the approach of independent vertical columns is used. Fourth, the parametrizations should be scale-independent, flexibly adapting to any NWP model domain, space and time resolution. Fifth, in the operational environment, the additional radiation calculations should be formulated optimally, in order to avoid a significant increase of the use of computing resources or the number of extra parameters and fields required.

Our formulation of the basic equations, accounting for the orographic effects on radiation, follows and develops the approach Müller & Scherer (2005). The main emphasis and novel formulations of our study are related to the way of application of the basic equations, and to processing of the high-resolution orography data for derivation of the required orographic parameters, that is, to the first, fourth and fifth requirements above. In our approach, the time-dependencies of some of the basic orography-related parameters are transformed to direction-dependencies. We apply the experience gained by developing HIRLAM parametrizations of the mesoscale and small-scale orography effects on momentum fluxes (Rontu, 2006).

This article aims at a systematic presentation and evaluation of the new orographic radiation parametrizations, as developed for and applied in HIRLAM (Sections 2–4). For completeness sake, the main properties of the basic HIRLAM radiation scheme are briefly summarized in the proper context. We report on a series of sensitivity studies, comparing the results of HIRLAM with the new parametrizations to those obtained by applying the basic radiation scheme alone (Section 5). However, the long-term verification of the suggested orographic radiation parametrizations in the operational NWP environment is postponed to subsequent studies. A general discussion of the requirements posed for radiation parametrizations of the mesoscale NWP models, as well as the validation of the basic HIRLAM radiation scheme, are also beyond the scope of this study. For the latter, the interested reader is referred to van Meijgaard et al. (2001) and Niemelä et al. (2001a,b).

2. Basic equations

Figure 1 shows the main SWR (Fig. 1a) and LWR (Fig. 1b) fluxes modified by the terrain features. The direct solar radiation is absorbed and scattered by atmospheric gases, aerosol and cloud particles and is reflected by clouds and the surface. Part of the scattered and reflected radiation reaches the (sloping) surfaces as diffuse radiation. Surrounding mountains and hills (as well as smaller-scale obstacles like rocks, trees, buildings and individual cumulus clouds, not discussed in the present study) create shadows and obscure parts of the sky visible at a given location. LWR is emitted and absorbed by the atmospheric gases, aerosol and cloud particles. Long-wave emission by sloping surfaces may significantly influence the surroundings and reduce net long-wave cooling especially in valley bottoms.

2.1. Direct solar radiation

The height of a location influences the intensity of downwelling solar radiation. In clear sky conditions, the higher the elevation is, the smaller is the optical thickness of the atmosphere above it. In satellite pictures, the high mountain areas show up as maxima of net SWR. This effect is taken into account already by the basic radiation parametrization, which knows the surface pressure and properties of the atmosphere above the location, calculating the attenuation of the downwelling SWR accordingly.

In HIRLAM, the clear sky global (direct + diffuse) downwelling solar radiation flux density perpendicular to the direction of the solar beam at the bottom of atmosphere ($S_{\downarrow 0}$) is parametrized according to Savijärvi (1990) as

$$S_{\downarrow 0} = S_o\Big[1 - 0.024\sin(h_s)^{-0.5} - c_{aa}0.11u_s^{0.25} - a_s\frac{p}{p_o}(0.28)/(1 + 6.43\sin(h_s) - 0.07\alpha)\Big], \quad (1)$$

where S_o is the solar flux at the top of atmosphere, h_s is the solar height angle, u_s denotes vertically integrated water vapour path (in cm), linearly scaled by pressure and divided by $\sin(h_s)$, and α is the surface albedo. The coefficients $c_{aa} = 1.20$ and $c_{as} = 1.25$ are related to absorption and scattering due to atmospheric

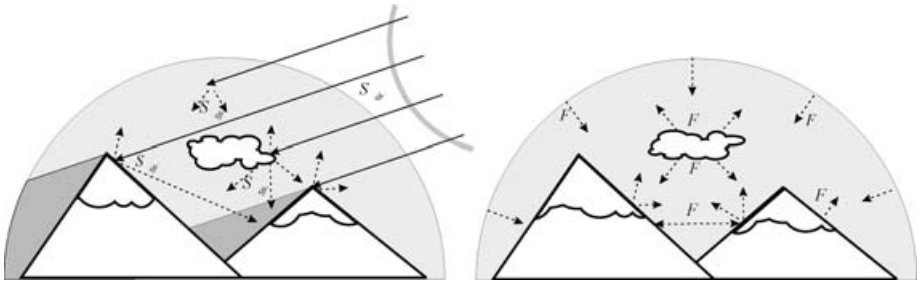

Fig. 1. Solar (short-wave) and terrestrial (long-wave) radiation fluxes over mountainous terrain: direct ($S_{\downarrow dr}$) and reflected by the clouds and surface ($S_{\uparrow df}$) and scattered by the atmosphere ($S_{\downarrow df}$, $S_{\uparrow df}$) solar radiation fluxes (a) and LWR fluxes emitted by the surface ($F_{\uparrow}$), clouds and atmosphere ($F_{\downarrow}$, $F_{\uparrow}$) (b). In the figure, sun is in the right upper corner and shadow-covered areas are shaded in dark.

aerosol, respectively. The first term in eq. (1), depending on solar height, describes the stratospheric absorption due to ozone, the second parametrizes the tropospheric absorption by water vapour, carbon dioxide and oxygen. The last term takes into account scattering of the downwelling solar radiation by the atmospheric gases and adds a compensating effect due to backscattering of the reflected beams. The aerosol effects are roughly estimated by multiplying the absorption and scattering terms by the coefficients c_{aa} and c_{as}.

The diffuse solar radiation arriving at the surface consists of SWR flux (1) scattered by atmospheric gases and aerosol particles, (2) transmitted through clouds and (3) reflected by the surface and multiply rescattered towards the surface. In HIRLAM, the diffuse SWR is determined as a sum of separately calculated clear sky and cloudy contributions:

$$S_{\downarrow df,0} = S_{\downarrow df,\text{clear}} + S_{\downarrow tr,\text{cloud}}, \tag{2}$$

where the clear-air diffuse radiation $S_{\downarrow df,\text{clear}}$ is approximated by an empirical formula based on Paltridge & Platt (1976),

$$S_{\downarrow df,\text{clear}} = \frac{d_1}{\sin(h_s)}[1 - \exp(-d_2 h_s)]. \tag{3}$$

The values of the empirical constants are $d_1 = 100$ W m^{-2}, $d_2 = 2.87$ (h_s is given in radians). The SWR flux transmitted through clouds $S_{\downarrow tr,\text{cloud}}$ is calculated using cloud short-wave transmissivity and absorptivity functions, defined as fits to a two-stream five-band radiative transfer model derived from Savijärvi et al. (1997) and Hu & Stamnes (1993). The functions depend on the solar height angle and the vertical integral of the cloud condensate content above a given level. The effective droplet radius, diagnosed from cloud condensate content according to empirical formulae, is calculated separately for water and ice clouds (Wyser et al., 1999).

The direct solar flux arriving at a slope in a certain direction is obtained by multiplying the incoming flux with the cosine of the angle n between the sun rays and normal of the surface (Fig. 2), for derivation see Kondratyev et al. (1978):

$$\cos(n) = \cos(h_m)\sin(h_s) + \sin(h_m)\cos(h_s)\cos(a_s - a_m), \tag{4}$$

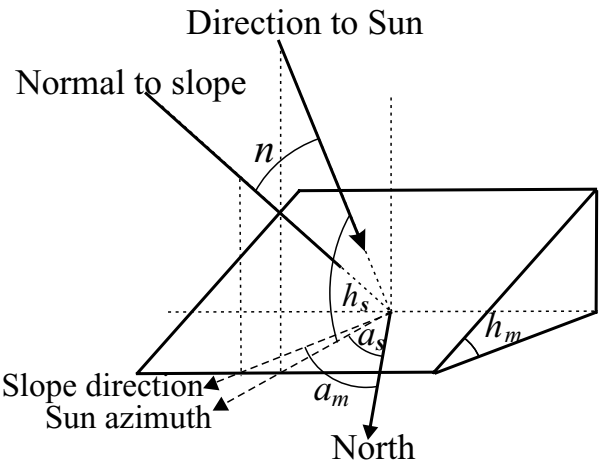

Fig. 2. Definition of the angles used in eqs (4) and (5).

where h_m is the slope height angle, a_m the aspect (downslope direction) angle and a_s is the solar azimuth angle (Fig. 2). The angles a_s and a_m are defined clockwise starting from geographic north and h_s and a_s at a given location depend on time and date of the year, according to standard astronomical formulae. Taking into account, that the area of a gridsquare at a sloping surface is larger than that at the level surface by a factor $1/\cos(h_m)$, we arrive at the slope factor in the form introduced by Müller & Scherer (2005),

$$\begin{aligned}\delta_{sl} &= \cos(n)/\cos(h_m) \\ &= \sin(h_s)[1 + \tan(h_m)/\tan(h_s)\cos(a_s - a_m)].\end{aligned} \tag{5}$$

The slope factor is used to modify the downwelling direct solar flux,

$$S_{\downarrow dr,1} = \delta_{sl} S_{\downarrow dr,0}, \tag{6}$$

where the unmodified downwelling direct solar flux is given by the difference between the global and diffuse SWR fluxes,

$$S_{\downarrow dr,0} = S_{\downarrow 0} - S_{\downarrow df,0}. \tag{7}$$

The slope factor at every gridpoint is a non-linear function of time and terrain elevation around the point. Over a level surface

($h_m = 0$), eq. (5) reduces to the simple relation $\delta_{sl} = sin(h_s)$, used by the basic radiation parametrization for the definition of SWR flux, $S_{\downarrow dr,1} = S_{\downarrow dr,0} \sin(h_s)$.

2.2. Self-shadowed surfaces and relief shadows

The side of an obstacle opposite to the sun is self-shadowed so that no direct solar radiation arrives there (Fig. 1). This effect is taken care by the formulation of eqs. (5)–(7). Relief shadows are created when the sun is below the local horizon, that is, when surrounding obstacles obscure the sky in the direction of the sun. Denoting the local horizon angle in a given geographical direction θ by $h_h(\theta)$, a shadow fraction δ_{sh} is defined, with values between 0 (shadowed) and 1 (clear) so that $\delta_{sh} = 0$ when $h_s < h_h(\theta)$ and $\delta_{sh} = 1$ when $h_s > h_h(\theta)$. This is a generalization of the binary shadow mask suggested by Müller & Scherer (2005). The direct solar radiation is now given by

$$S_{\downarrow dr,2} = \delta_{sh} S_{\downarrow dr,1}. \tag{8}$$

With the exception of deep valleys, the relief shadows are only important when the sun is close to the horizon and, consequently, the intensity of downwelling SWR is small. Thus this effect is expected to be minor.

2.3. Diffuse and reflected radiation over complex terrain

At a given location, diffuse solar radiation comes from the visible sky restricted by the local horizon. A sky-view factor (SVF) δ_{sv} (Müller & Scherer, 2005) is defined by integration of the horizon angle $h_h(\theta)$,

$$\delta_{sv} = 1 - \frac{1}{2\pi} \int_0^{2\pi} \sin[h_h(\theta)]\, \mathrm{d}\theta. \tag{9}$$

The values of δ_{sv} vary from 0 (no sky seen) to 1 (the whole sky visible).

In addition, the SWR reflected by the surrounding terrain is accounted for. Thus, the flux of diffuse radiation is approximated by

$$S_{\downarrow df,1} = \delta_{sv} S_{\downarrow df,0} + \alpha_e (1 - \delta_{sv}) S_{\downarrow,e}, \tag{10}$$

where α_e is the average surface albedo and $S_{\downarrow e}$ the average downwelling global radiation over the surrounding surfaces. During the actual calculations, values over the surroundings are approximated by the flat surface values [$\delta_{sl} = \sin(h_s)$] at the central point, that is, $\alpha_e \approx \alpha$ and $S_{\downarrow e} \approx \sin(h_s)\,(S_{\downarrow dr,0} + S_{\downarrow df,0})$.

2.4. Terrain-modified net short-wave radiation

The net SWR flux is conveniently defined as the difference between the global downwelling and reflected fluxes, $S_{\text{net}} = S_{\downarrow} - S_{\uparrow}$. As the orographic radiation parametrizations only modify the downwelling fluxes, we define the upwelling SWR flux as $S_{\uparrow} = \alpha S_{\downarrow,0}$. Combining this with eqs. (6), (8) and (10), we arrive at an equation for the net SWR over complex terrain:

$$S_{\text{net}} = [\delta_{sl}\delta_{sh} - \alpha\delta_{sv} \sin(h_s)] S_{\downarrow dr,0} + [(1 - \alpha)\delta_{sv}] S_{\downarrow df,0}. \tag{11}$$

According to eq. (11), the orography effects on the surface net SWR are obtained by multiplying the direct and diffuse radiation, produced by the basic radiation scheme, by the slope factor, shadow fraction and sky-view factor. Over a flat surface [$\delta_{sl} = \sin(h_s)$, $\delta_{sh} = \delta_{sv} = 1$], eq. (11) reduces to the basic $S_{\text{net}} = (1 - \alpha)(S_{\downarrow dr,0} + S_{\downarrow df,0})$.

2.5. Long-wave radiation

The HIRLAM LWR parametrization uses a broad-band emissivity scheme in a local isothermal approximation. The water vapour line emissivity is a function of integrated water vapour content; water vapour continuum, carbon dioxide and ozone effects are added as extra terms (Savijärvi, 1990; Räisänen et al., 2000). Cloud effective emissivity depends on cloud water and ice amounts and on an empirically defined effective radius of water droplets and ice crystals (Wyser et al., 1999). Downwelling LWR flux below the cloud base $F_{\downarrow 0}$ is calculated as a combination of contributions from clear-sky and cloud-covered parts. Upwelling LWR is determined by the surface emissivity and temperature.

Downwelling LWR arriving at a given location is emitted by the clear or cloudy sky, restricted by the sky view and partly emitted by the surrounding slopes and obstacles above the horizon, following the formulation by Müller & Scherer (2005):

$$F_{\downarrow} = \delta_{sv} F_{\downarrow 0} + (1 - \delta_{sv}) F_{\uparrow 0,e}, \tag{12}$$

where σ is the Stefan-Boltzmann constant, $F_{\uparrow 0,e} = \epsilon_e \sigma T_{se}^4$, ϵ_e is the average surface emissivity and T_{se} the average surface (skin) temperature of the surrounding terrain. During the actual calculations, it is again assumed that the surface properties in the gridpoint and its environment are similar, $T_{se} \approx T_s$ and $\epsilon_e \approx \epsilon$.

The net LWR flux is defined as $F_{\text{net}} = F_{\downarrow} - F_{\uparrow}$. Combination with eq. (12) leads to a simple expression for the orographically modified net LWR flux: $F_{\text{net}} = \delta_{sv}\ F_{\text{net},0}$. The smaller δ_{sv} is, the smaller is the absolute value of $F_{\text{net},0}$. Thus, the long-wave cooling should be smaller in the valleys and larger at the mountain tops. Effectively, the LWR fluxes in the valleys are assumed to balance mutually in all directions, except towards the sky.

3. Derivation and use of the orographic factors

As described above, the orographic correction of the surface radiation fluxes is obtained knowing three basic quantities: the slope parameter δ_{sl}, shadow fraction δ_{sh} and sky-view factor δ_{sv}. In order to fulfil the requirements posed in Introduction, that is, to use the most detailed orography information available and to

ensure the scale-independence, these parameters or their components are calculated in the grid of a high-resolution digital elevation data set. Parameter values for each gridpoint of the required HIRLAM domain and resolution are aggregated from the high-resolution values. Aggregation is done as a part of the preparation of physiography description data for the model of given resolution and integration domain. Time-dependent information is taken into account during the actual forecast run only.

In this study, orography calculations were based on the HYDRO1k elevation derivative data base from U.S. Geological Survey (USGS, 2003). It provides 1-km-resolution data of global coverage (excluding Antarctica and Greenland) of terrain elevation, together with the derived slope and aspect angles, etc., given in an equal area azimuthal Lambert projection. HYDRO1k is derived from the Global 30 arcs elevation data set (GTOPO30", USGS (1998)). However, our method of calculation of the orographic parameters for radiation is, in principle, independent of the choice of the source data.

3.1. Slope parameter

The slope parameter defined by eq. (5) contains solar height and azimuth angles in combination with slope and aspect angles. The former depend on time and location, while the latter are functions of the location only. To avoid preprocessing and storage of large amounts of time-dependent data while still retaining essential details of the orography, the concept of slope fractions is introduced. Within each HIRLAM grid square, slopes given by the high-resolution source data are classified into directional sectors, according to where they are facing to. Mean slope angle within each sector and fraction of data points in each sector are calculated. During the actual forecast run, when the solar height and azimuth are known, an integrated slope factor for each gridpoint is calculated as a weighted sum of the sector values. Eq. (5) can now be reformulated as

$$\delta_{sl} = \sin(h_s) + \cos(h_s) \sum_{i=1}^{8} f_i \tan(h_{m,i}) \cos(a_s - a_{m,i}), \quad (13)$$

where f_i is the fraction and $h_{m,i}$ the mean height angle of the slopes in each sector i, centred at (8) azimuth angles $a_{m,i} = 0^\circ$, $45^\circ, \ldots, 270^\circ, 315^\circ$ (N, NE, E, SE, S, SW, W, NW-note that the sum of fractions may be less than one because flat terrain does not contribute). At each HIRLAM gridsquare we thus get two new arrays, each with eight members. In case of a homogeneous environment and fine model resolution, one of the sectors will dominate. On the contrary, in a coarse-resolution grid, the effects of different slopes are expected to cancel each other, with the grid-averaged result well described by the flat surface approximation. Note that the first right-hand side term $[\sin(h_s)]$ in eq. (13) is taken care of by the basic radiation parametrizations, so that only the slope correction needs to be added here.

3.2. Local horizon, shadow and sky-view factors

At each high-resolution orography source data (HYDRO1k) point, a local horizon angle $h_{h,i}$ is calculated for the same (8) directional sectors. The horizon is scanned, with a high resolution, in a circle around the location. In this study, we restricted the radius of the circle to 20 km, scanning it with a resolution of 1°. The local horizon angle is determined by the elevation difference and distance between the central and the surrounding points. Each angle is weighted according to its squared distance from the central point. Thus the closest obstacles, which are able to obscure the largest area, get more weight than the remote ones. At each point, the sectorial local horizon angles $h_{h,i}$ are defined by the weighted average of the 1° values.

For the calculation of the shadow factor, minimum and maximum values of $h_{h,i}$ are found in each sector. Direction-dependent coefficients A_i and B_i are determined so as to fulfil a linear relationship

$$\delta_{sh,i} = A_i \sin(h_s) + B_i, \quad (14)$$

assuming that $\delta_{sh,i} = 1$ when $h_s > h_{h,i,\max}$ and $\delta_{sh,i} = 0$ when $h_s < h_{h,i,\min}$. Between the minimum and maximum values, $\delta_{sh,i}$ is assumed to increase from zero to $1 - b_{\rm cr}$, where $b_{\rm cr}$ is taken to be $1/N$ and N is the number of HYDRO1K points inside a HIRLAM gridsquare. During the actual HIRLAM run, the precalculated coefficients are inserted to eq. (14) for computation of the time-dependent shadow factor $\delta_{sh,i}$, due to the obstacles in the sector of the current solar azimuth.

The sky-view factor is used for calculation of the LWR and diffuse SWR. At each high-resolution data point, SVF is obtained by integration over the local horizon angle, determined by the nearby orography (eq. 9). Here the integration is replaced by summation of the sectorial local horizon values $h_{h,i}$,

$$\delta_{sv} \approx 1 - \frac{\sum_{i=1}^{8} \sin(h_{h,i})}{8}. \quad (15)$$

The grid-scale δ_{sv} is obtained as an average of the fine-resolution SVF values. Note that we use, for simplicity, the values of $h_{h,i}$, representing quite large area around each fine-scale gridpoint. This results in certain smoothing of the grid-scale δ_{sv}.

4. Modified algorithm of radiation calculations

After the modifications, the radiation calculations at each time step at each HIRLAM gridpoint are organized as follows:

(i) Use the astronomic formulae to calculate the time-dependent solar height and azimuth angle, based on time, date and position (latitude, longitude).

(ii) Calculate the gridsquare-averaged albedo, emissivity and skin temperature, based on the values of surface subtype temperature, albedo, emissivity and snow cover provided by the surface description, analysis and parametrizations.

(iii) Call the main radiation scheme to calculate the radiative temperature tendencies and fluxes, assuming the surface is flat and homogeneous. To calculate the upwelling fluxes, grid-square averaged surface elevation, albedo, emissivity and skin temperature are used.

(iv) Use the precalculated orography parameters: directional fraction of slopes and slope angle in each direction (Section 3.1), directional coefficients and the average SVF (Section 3.2), to update the downwelling SWR and LWR fluxes over the uneven terrain.

(v) Calculate, within the surface parametrization scheme, the SWR and LWR net fluxes for each surface subtype, using results of (iv) together with the subtype-specific albedo and emissivity values. The net fluxes are used for calculation of surface energy balance over the surface subtypes.

This procedure ensures a consistent combination of the radiation and surface parametrizations, descending from the (grid-averaged) atmospheric radiation parametrizations to the mesoscale features (represented by the subgrid-scale orography) over heterogeneous surface (represented by the radiative properties of the surface subtypes).

The original HIRLAM radiation scheme was designed to be quick and simple, yet provide results accurate enough for a short-range NWP model. The increase in computational resources due to the added orography-related parametrizations is insignificant: about one percent of CPU time plus the space needed by the several new two-dimensional, time-independent arrays of the orographic parameters. This allows, in contrary to some radiation schemes of the operational NWP models, to continue performing full radiation calculations at each time step during the model integration. This is considered to be important for maximum accuracy in handling the cloud–radiation interactions. The time consumption during the physiography generation phase, when the necessary orography-related parameters are calculated (once) for a given model resolution and domain, is larger but acceptable.

5. Effect of the improved parametrization

In the next subsections, four different types of comparison studies are presented and discussed. Scales of the time-independent orography-related parameters are first illustrated in Section 5.1. The possible magnitude of orographic effects on radiation fluxes is then estimated with a stand-alone, single-column radiation scheme without integration in time (Section 5.2). Next, the sensitivity of the surface energy balance, near-surface temperature and humidity conditions to the changes of radiation fluxes is analysed in the framework of time-dependent, single-column experiments, which include all physical parametrizations of HIRLAM (Section 5.3). Comparison of the full three-dimensional model experiments, using model setups of two different horizontal resolutions over the Carpathian mountains (Section 5.4) concludes the sensitivity studies.

5.1. Scales of the orography-related parameters

To ensure the scale-independence of the parametrization scheme, the basic orographic parameters should behave consistently when the model's resolution is altered. With increasing resolution, more details should become visible (i.e. variance should increase) while the area-averages should remain unchanged.

Figure 3 shows values of the calculated SVF over the Carpathian mountains. The factor varies from 0.92 to 1 in the coarse-resolution setup (with model's horizontal grid-size $\Delta x =$ 33 km), while it lays between 0.84 and 1 in the finest-resolution ($\Delta x = 1.7$ km) model. In all cases, however, the mean value of this parameter over the area shown in Fig. 3 is about 0.975 (Table 1). The variance does not increase much towards the finest scales because of the inherent smoothing in the calculation of δ_{sv} (see Section 3.2). Note also that in practice, the maximum SVF is unity.[1] Thus, even in the coarse-resolution setup, the area-averaged SVF is smaller over mountains than over flat areas, and the related mean effect is non-zero. The values of the mean slope are seen to behave in a similar way: maximum values and variance increase with increasing resolution, but the average values change only little (Table 1). These comparisons and those for the time-dependent parameters (not shown) allow us to conclude that the aggregation of the orographic parameters is made correctly.

5.2. Standard tests on radiation fluxes

Standard temperature and humidity profiles for mid-latitude summer and winter defined in "Intercomparison of Radiation Codes used in Climate Models" (ICRCCM, Ellingson & Fouquart, 1991) were used in one-dimensional HIRLAM experiments. All gases and aerosols were included. Low clouds with a cloud condensate content 105 g kg^{-1} were assumed to lie at the level of 1.5 km (802 ... 902 hPa) and the high clouds at 5 km (487 ... 554 hPa). In addition, a surface inversion was created for the LWR comparison, by modifying the ICRCCM mid-latitude winter profile so that the surface temperature became 10° colder than the air at the 1-km height.

Figure 4 illustrates the slope effect on downwelling global SWR. The radiation flux arriving at northern, eastern, southern and western slopes was calculated and compared with the flux on a plane surface. Clear sky, mid-latitude winter profile, date 21 March, latitude 55 N, longitude 0 E and slope angles of 25° define the SWR flux at plane surface. Note that we assumed quite large slope angles in order to illustrate the maximum possible effects. The difference between the maximum (southern slope) and minimum (northern) values reaches 700 W m^{-2}. The maximum downwelling flux at the eastern and western slopes

[1] At the top of the highest mountains, possibly $\delta_{sv} > 1$. However, with the present resolutions of the orography source data and the model grid, such values were not obtained.

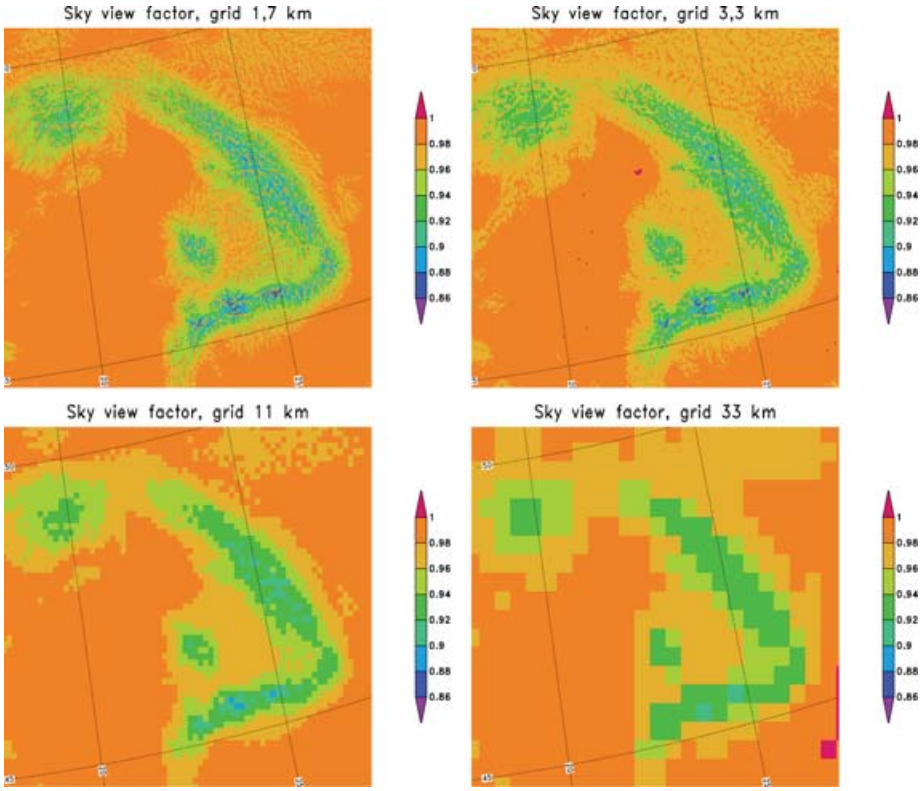

Fig. 3. Sky-view factor as seen by HIRLAM setups with a horizontal resolution Δx of 1.7 km (a), 3.3 km (b), 11 km (c) and 33 km (d).

Table 1. Statistical characteristics of the sky view factor (0. . .1) and mean slope (°) over Carpathian mountains with different model resolutions. σ denotes standard deviation.

Parameter	Δx (km)	Minimum	Maximum	Average	σ
SVF	1.7	0.841	1.0	0.974	0.019
	3.3	0.854	1.0	0.974	0.021
	11.1	0.890	1.0	0.974	0.018
	33.3	0.915	1.0	0.976	0.019
Gridsquare	1.7	0.0	22.9	1.76	2.29
mean slope	3.3	0.0	20.3	1.75	2.05
	11.1	0.0	10.7	1.73	1.85
	33.3	0.0	8.5	1.67	1.65

is almost equal,[2] but the eastern slopes reach the maximum 4 h earlier than the western ones. These differences are due to the slope effect, controlled by the slope factor (eq. 5) and correspond to those observed at sloping surfaces (see e.g. Müller & Scherer, 2005, and references therein).

The influence of diffuse radiation is seen most clearly when the direct solar radiation does not reach the slope, that is, in the morning over the western and in the evening over the eastern slopes. Maximum about 60 W m^{-2} of diffuse radiation arrives there during the first and last 3 h of day. The effect of the assumed relief shadows leads to a decrease of the maximum downwelling solar radiation flux by about 100 W m^{-2} approximately 1 h after the sunrise on the eastern, and 1 h before the sunset on the western slopes.

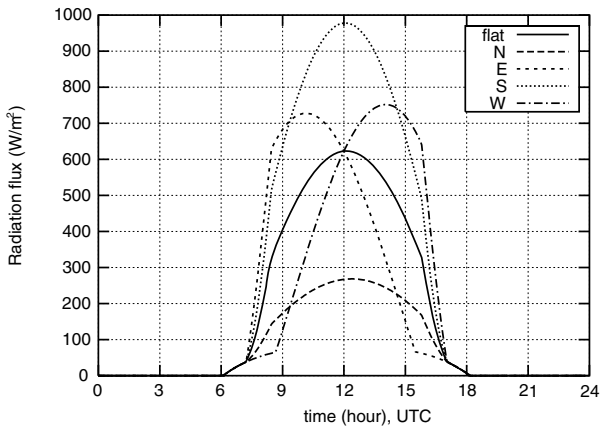

Fig. 4. Time-evolution of downwelling global SWR at 21 March, location 55 N, 0 E, over level surface (flat), at northward (N), eastward (E), southward (S) and westward (W) facing slopes. Slope height angle 25°, mid-latitude winter atmospheric profile, SVF $\delta_{sv} = 1$. Cast shadow is assumed to appear ($\delta_{sh} < 1$) at solar height angle $h_s = 20°$ and cover the whole area ($\delta_{sh} = 0$) below $h_s = 10°$. Time given in UTC.

[2]Note that UTC, not the local solar time, was used in the calculations. This leads to the slight asymmetry of the curves.

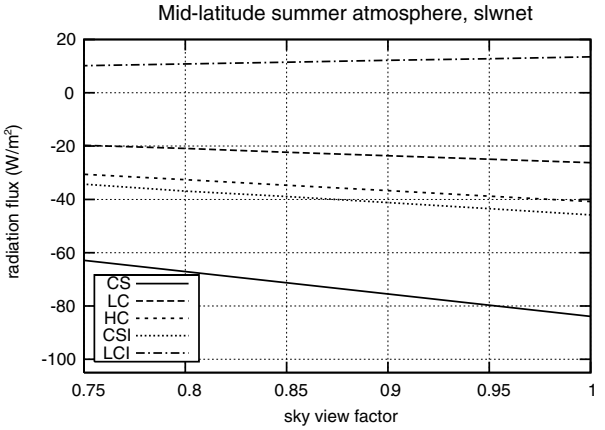

Fig. 5. Net LWR flux at surface as a function of SVF. Clear sky conditions (CS), low (LC) and high (HC) clouds, with the standard mid-latitude summer conditions; clear sky (CSI) and low clouds (LCI) with surface inversion. Emissivity of the surrounding terrain = 1, cloud cover 6 octas = 75%.

The effect of SVF on global SWR in clear and cloudy cases was studied in the same mid-latitude equinox conditions. The clouds were assumed low, with full cloud cover. Decrease of the SVF by 15% decreases the downwelling short-wave clear-sky global radiation only by ca. 5%, when the albedo of surrounding terrain is assumed to be 0.5 (a realistic value for spring-time snow cover). The difference between clear and cloudy sky situations is much larger. When low clouds are added, the global radiation flux decreases to ca. 100 W m^{-2} from the maximum value of 700 W m^{-2}. In the cloudy case, the flux consists only of the diffuse radiation, which is reflected from the surrounding surfaces and influenced by the SVF according to eq. (10).

Dependency of the orographically modified LWR on the sky view factor (Section 2.5) was studied in clear-sky and cloudy cases, with and without surface inversion. The net long-wave flux at the surface increases with decreasing SVF both in the cloudy (with low and high clouds) and clear-sky cases, except when there are low clouds and inversion (Fig. 5). As expected, the long-wave cooling is strongest in the clear-sky conditions and SVF equal to one. SVF decrease of 15% leads to decrease of the cooling by ca. 10 W m^{-2}. In the cloudy inversion case the net LWR flux is almost constant and tends to heat the near-surface air.

5.3. *Near-surface variables predicted by the single-column HIRLAM*

In these experiments, modelled vertical profiles of temperature, humidity and cloud water representing early spring conditions in Sodankylä (67° 22N 26° 39′E, WMO station number 02836, northern boreal forest at the altitude of 179 m, without significant hills or mountains nearby) were used as an initial state of a 24 h integration with a single-column version of HIRLAM. The experiment was started at 00 UTC, corresponding to about

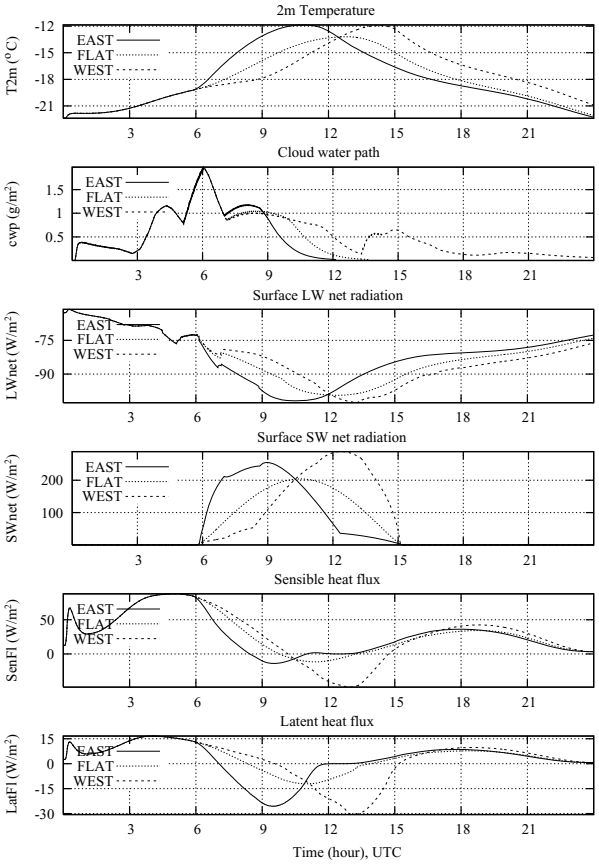

Fig. 6. Time-series of single-column model output for artificial eastern and western slopes compared with a flat simulation in Sodankylä 1 March 2005. Parameters and line definitions are shown in the inserted titles and legends, time in UTC. Fluxes are denoted positive towards the surface.

01:40 local solar time. In the single-column setup, all physical parametrizations of the model were active while the horizontal advection of the model variables was replaced by an assumed weak geostrophic advection (3 m s^{-1}) and zero large-scale vertical velocity. In addition to the control (flat) case, experiments were performed with artificial eastward and westward directed slopes of 22°. In all experiments, the location was assumed unshadowed and sky view unrestricted, with surface albedo of 0.6 (snow-covered forest). The aim of the experiment is to detect the possible effects of orographically modified radiation fluxes to the latent and sensible heat fluxes, as well as to the near-surface temperature and humidity conditions.

Figure 6 shows an example of time-series of the net SWR and LWR, sensible and latent heat fluxes, screen level temperature and cloud water path (vertically integrated cloud condensate content) for the spring simulation. The net radiation fluxes behave as expected: more SWR arrives at the eastern slope in the morning and at the western slope in the evening. The maximum 2-m temperature is 2° higher (−12 °C versus −14 °C) and maximum 2-m

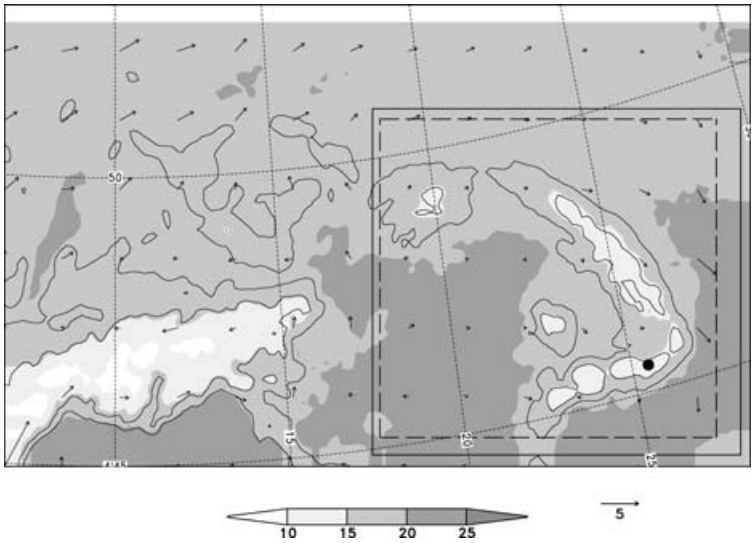

Fig. 7. Experiment domains over the Carpathian mountains: whole area—11 km-resolution area, full-line box—3.3 km-resolution area, dashed-line box—comparison area. Solid lines: 500 m and 1000 m isolines of mean surface elevation as seen by RR11; shaded: analyzed 2-m temperature of RR11, averaged in time between 1 June 00 UTC and 7 June 00 UTC, 2000, scale as shown; wind vectors: averaged over the same period 10-m wind based on +06 h forecasts of RR11, scale given by the 5 m s^{-1} arrow below the figure. Location of the mountain station VF Omu (WMO number 15280, 25.45E, 45.45N) is shown by a dot in the southeast part of the map.

specific humidity about 0.15 g kg^{-1} larger (1.37 g kg^{-1} versus 1.22 g kg^{-1}, not shown) over the slopes than in the control case. Maximum values of the sensible and latent heat fluxes from surface to atmosphere occur slightly earlier than the temperature and humidity maxima. There are differences of temperature, humidity and turbulent kinetic energy profiles especially in the lowest 500 m layer above the surface (not shown).

The behaviour of the vertically integrated cloud condensate shows interesting features. In all cases a thin cloud layer forms at the 1500 m level during the first hours of integration (vertical profile not shown). In the control and eastern simulations, the cloud dissolves during the afternoon. In the western simulation, the cloud starts to grow again in the afternoon and remains till the evening. Note that the Sodankylä observations indicated good visibility and no low clouds over the whole period (but diamond dust was observed at the station at 00 UTC). Also the operational HIRLAM did not predict low clouds or fog in this case. However, we could conclude that in sensitive cases, the orography-induced differences of radiation fluxes may influence in cloud formation in the model, with feedback to the radiation fluxes. Correspondingly, a summer simulation (not shown) indicated triggering of convection in otherwise cloudless cases when slope radiative effects were included.

5.4. *Model comparisons in an anticyclonic case over the Carpathian mountains*

We now turn to full three-dimensional model simulations with or without parametrization of orographic effects on radiation. The aim of these experiments is to reveal the sensitivity of the model in a real situation. We seek answer to questions like: Are there local effects on forecasted parameters? Can we see interactions between radiation, temperature and clouds? Is it possible to detect any larger-scale effects? What is the influence of model's horizontal resolution? Comparison with observed 2-meter temperature at one station is included in order to see how close to reality the results of the new parametrizations are.

Simulations with HIRLAM (v. 6.4.3) with horizontal resolutions of 11 and 3.3 km with (experiments RO11 and RO03) and without (experiments RR11 and RR03) the orographic radiation parametrizations were run over the Carpathian area (Fig. 7). In the nested setup, analyses obtained from the larger-scale experiments define the lateral boundaries for the finer-scale experiments. For the 11-km experiment, 33-km resolution HIRLAM 6.2.0 reanalysis data were used as boundaries. In all experiments, the number of levels in the vertical was 40. Three-dimensional variational data-assimilation was applied in a cycle of 6 h. Thirty-six-hour-long forecasts were started at 00 UTC and 12 UTC only. A week in the beginning of June 2000, with prevailing anticyclonic weather and mainly cloudless sky over the area, was chosen for the experiment. For the analysis of results, RR11 and RO11 data were interpolated to the grid of RR03 and RO03, with minimum loss of accuracy because of using the fine-resolution grid as common framework.

Differences of the energy fluxes, temperature and clouds between the 3.3 km-resolution experiments may be significant at mountains. For example, at the station VF Omu (see Fig. 7 for the location), the maximum difference of downwelling global radiation flux are 150–200 W m^{-2} (Fig. 8a). During the morning hours, the difference is due to the slope effect: more solar radiation arrives at the gridpoint where the slope is directed to east. The related maximum temperature difference is almost 3 K (Fig. 8b). Towards the afternoon, cloud condensate content grows more in the experiment with orographic radiation parametrizations (RO03) than in the reference one (RR03). The difference leads to a negative difference in the direct SWR flux, partly compensated by the positive difference in LWR and diffuse SWR. The surface energy balance (the sum of turbulent sensible and

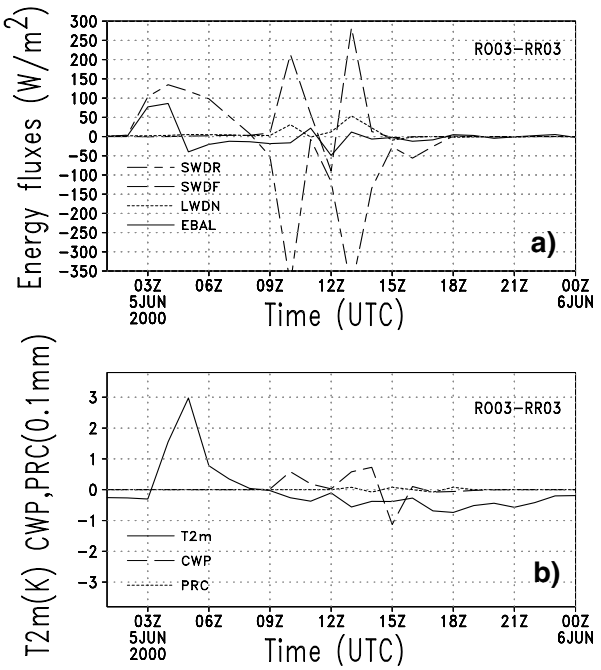

Fig. 8. Time-evolution of the difference between (a) downwelling radiation fluxes: direct (SWDR) and diffuse (SWDF) SWR, LWR (LWDN) and surface energy balance (EBAL), all in Wm^{-2}, (b) 2-m temperature (T2m, K), vertically integrated cloud condensate content (CWP, 0.1 mm) and hourly precipitation rate (PRC, 0.1 mm), predicted by the experiments RO03 and RR03. The time-series are defined by the hourly output of the model runs starting from the analysis of 5 June 2000 at 00 UTC, and represent the nearest gridpoint to the high-mountain station VF Omu (Fig. 7). Denotation of the lines is shown in the inserted legends, forecast times are given in UTC.

latent heat fluxes plus net SWR and LWR), predicted by RO03, is larger in the morning and somewhat smaller in the afternoon, than that of RR03. Precipitation is insignificant during this day.

Mean differences between the experiments over the entire mountain area are small. The averaged global downwelling radiation of RO03 is slightly larger in the morning and slightly smaller in the afternoon than in RR03. During the late morning, the averaged diffuse radiation increases somewhat more in RO03 than in RR03. Over the flat areas, and also averaged over the whole domain, the differences are insignificant. Thus, at least in this particular case, the orographic effects on radiation remain local. As expected, the comparison between the 11 km-resolution experiments revealed only minor differences. The variance of the forecasted parameters in the coarse-resolution experiments was one order of magnitude smaller than in the fine-resolution experiments.

Figure 9 illustrates the distribution of temperature and cloud differences between RO03 and RR03 over the comparison area at different times of day: morning, afternoon, night. All maps are based on +5h forecasts starting 4th June at 00, 12 and 18 UTC, valid at 06:43, 18:43 and 00:43 local solar time, respectively. The maximum differences are within $\pm 50\ \mathrm{W\,m}^{-2}$ for net radiation fluxes (not shown), $\pm 2^{\circ}$ in screen level temperature, $\pm 0.5\ \mathrm{kg\,m}^{-2}$ for vertically integrated cloud condensate. The contours of the Carpathian mountains can be distinguished, especially from the (almost cloudless) morning figure with warmer surfaces at the eastern, colder at the western slopes. In the afternoon, differences in cloudiness become visible. The shift of location of the individual weak convection cells at a given time, indicated by the figure, may also be due to other (random) effects than differences in radiation parametrizations. During night, the clouds and related differences again disappear. The local nighttime temperature differences are related to the LWR in locations with restricted sky view. The cold spot over the Bihor Mountains (Western Carpathians, in the middle of the map) seems to be related to the daytime cloud differences there. All differences remain close to the mountains, with some exceptions related to clouds.

Figure 10 brings us closer to reality. Here, the predicted by RR03 and RO03 2-m temperatures during the five first days of June, 2000 are compared with observed temperatures at VF Omu. There is a systematic difference of 6°–10° between the observed and predicted temperatures, both during day and night, except during the last two nights of the period. Introduction of the sloping surface radiation parametrizations does not essentially change the picture.

The key to understanding this discrepancy lies in the fact that the real height of the station is 2504 m above sea level, while the mean height over the corresponding gridsquare of the 3.3-km experiments is 1405 m, that of the 11-km experiments is 1257 m. The surface data assimilation system is not able to utilize the temperature observation of this (and another Carpathian high-mountain station) because the difference between the model's first guess surface temperature and the observed value is too large. Possibly the observed temperature differs too much also from that observed at neighbouring (low level) stations. The initial surface temperature of each forecast is already as incorrect as the forecasted values later. In the model, there is no mechanism to correct this temperature during a single forecast cycle.

In this case, the observation and gridbox mean value represent quite different environments, even within this high-resolution model setup. This example shows that in the NWP system over the mountains there may be sources of uncertainties leading to order-of-magnitude larger errors than possible improvements due to the advanced parametrizations. The different environments create problems also for verification of the forecast results over complex orography.

Finally, the Carpathian experiments described above, were repeated with a different HIRLAM version (v. 7.1alpha1), also excluding the parametrization of relief shadows ($\delta_{sh} = 1$, results not shown). In this case, exclusion of the relief shadows had almost no influence in the results. In addition, differences between the two HIRLAM versions in the parametrization of the moist

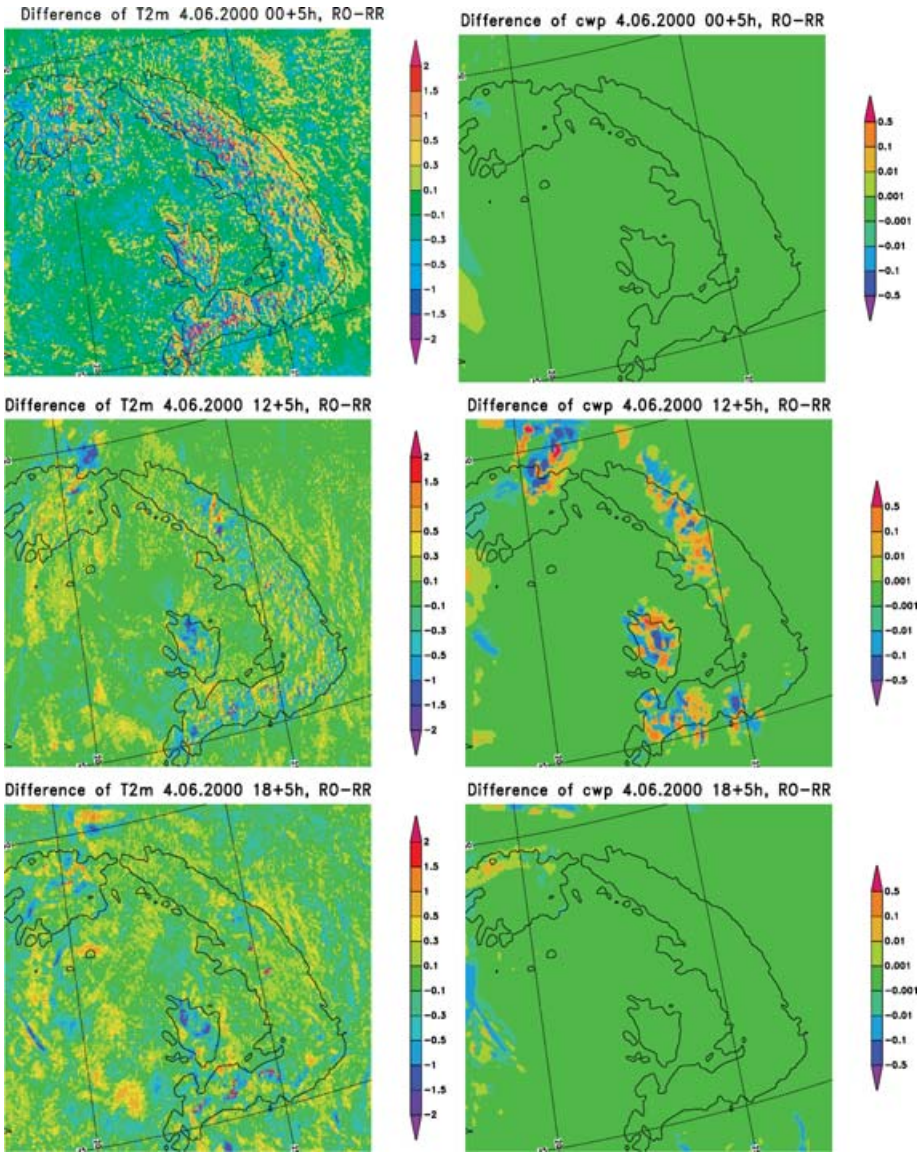

Fig. 9. Differences in temperature (left column, unit K) and vertically integrated cloud condensate (right column, unit kg m^{-2}) between RO03-RR03 in the morning (upper row), afternoon (middle row) and night (lower row), at 4 June over Carpathian mountains. Colour scales are shown on the right of each figure. Solid line shows the 500 m isoline of surface elevation.

processes, led to changes in the details of cloud formation, but did not change the general picture.

6. Conclusions and outlook

A parametrization scheme of subgrid-scale orographic effects on surface radiation fluxes was introduced to and evaluated in the High Resolution Limited Area Model (HIRLAM). In the formulation of the basic equations, the approach by Müller & Scherer (2005) is applied and developed. In preprocessing of the fine-scale orography information, we use methods developed for the parametrizations of mesoscale and small-scale orography effects in HIRLAM (Rontu, 2006). The basic orographic parameters—slope, shadow and sky-view factors—were derived from fine-resolution digital elevation data and aggregated to the model grid. The concept of directional fractions was formulated to convert the time-dependencies of the parameters to direction-dependencies. At each time step of the forecast, the time-independent orographic parameters are combined with those describing the changing solar position. This approach keeps the calculations computationally affordables both during the preprocessing and model preprocessing. More generally, the method allows a flexible and consistent exploitation of the finest-resolution orography data within model setups of different resolution and domain.

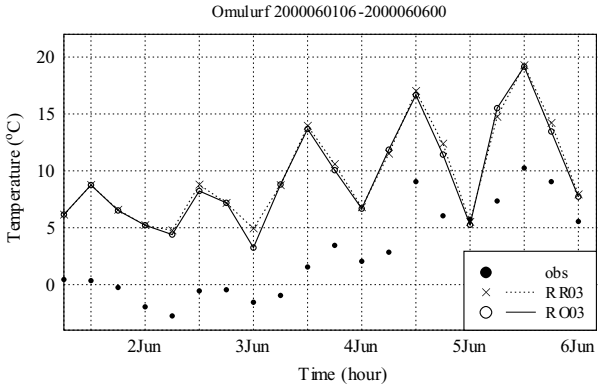

Fig. 10. Time-series of observed and predicted by RR03 and RO03 2-m temperatures at station VF Omu (WMO number 15280, location shown in Fig. 7).

Single-column experiments revealed quite large sensitivity of the model to the new parametrizations, especially via possible cloud–radiation interactions. In a real case study over the Carpathian mountains, local temperature and cloud effects were found in the finest-scale (3.3-km horizontal resolution) experiments. The largest local temperature differences of 1°–3° were due to the slope effect on the SWR during morning and late afternoon hours. Long-wave effects of somewhat smaller magnitude were detected during clear nights in locations with restricted sky view. In the coarser-resolution experiments (11 km-horizontal resolution), the differences were small, as were also the area-averaged effects in the fine-scale experiments. At a high-mountain station, differences between the predicted and observed 2-m temperature of one order of magnitude larger than the differences between predicted by the reference and modified radiation parametrizations, were detected. The large error seems to be related to the use of smoothed mean orography in combination with the surface data assimilation system of HIRLAM.

Based on this study, we cannot yet conclude that a significant improvement of the forecast is achieved by the introduction of the suggested parametrizations. A longer-term verification of the scheme against radiation and temperature observations over selected mountain areas is necessary before its operational implementation. This non-trivial task may require further development of the surface data assimilation and verification methods used in HIRLAM.

There are several possibilities to develop the suggested parametrizations. For example, calculation of the sky-view factor might be improved, to obtain less smoothed values for the finest-resolution models. Also, it would be interesting to see if the use of much higher resolution surface elevation data would influence the values of orographic and forecasted parameters. Such data are available also for the Carpathian region of the present sensitivity experiments.

The general question about the relative importance, in the short-range mesoscale NWP models, of (1) an accurate parametrization of the clear-sky radiative transfer, (2) cloud–radiation interactions and (3) surface-radiation effects, requires further research. A possible way to address this question is to compare, within a mesoscale NWP, the forecasted surface energy balance over complex terrain, as obtained using a detailed (e.g. European Centre of Medium Range Forecasts model) and a simple (e.g. HIRLAM) radiation scheme, with and without parametrization of the orographic effects on radiation, possibly with different parametrizations of cloud and soil-surface processes, which interact with the radiation parametrizations. The various spatial assumptions, related to cloud and radiation parametrizations (three-dimensional/one-dimensional approach), could be analysed in such a comparison study. Finally, the important aspect of the possible dynamical feedbacks, that is, the connection between radiation fluxes, temperature and local circulations, requires evaluation with respect to the wind and pressure observations.

7. Acknowledgments

Our thanks are due to the anonymous reviewers and David Schultz for valuable comments and advice, which helped us to clarify the main concepts and improve the readability of the manuscript. This study was supported by the mobility and network grants of the Nordic Research Board (NordForsk).

References

Dubayah, R. and van Katwijk, V. 1992. The topographic distribution of annual incoming solar radiation in the rio grande river basin. *Geophys. Res. Lett.* **19**, 2231–2234.

Ellingson, R. G. and Fouquart, Y. 1991. The intercomparison of radiation codes used in climate models: an overview. *J. Geophys. Res.* **96**, 8925–8927.

Hu, Y.-X. and Stamnes, K. 1993. An accurate parameterization of the radiative properties of water clouds suitable for use in climate models. *J. Clim.* **6**, 728–742.

Kondratyev, K. Y., Pivovarova, Z. and Fedorova, M. P. 1978. *The Radiation Regime of Sloping Surfaces*. Hydrometeoizdat, 216 pp. (In Russian).

Liang, X.-Z., Xu, M., Choi, H. I. L., Kunkel, K. E., Rontu, L. and co-authors. 2006. Development of the regional climate-weather research and forecasting model (CWRF): treatment of subgrid topography effects. Available as http://www.mmm.ucar.edu/wrf/users/workshops/WS2006/abstracts/Session07/7_3_Liang.pdf.

Matzinger, N., Andretta, M., Gorsel, E. V., Vogt, R., Ohmura, A. and co-authors. 2003. Surface radiation budget in alpine valley. *Quart. J. Roy. Met. Soc.* **129**, 877–895.

Müller, M. D. and Scherer, D. 2004. A radiation parameterization of topographic effects for mesoscale models. *Geophysical Research Abstracts. European Geosciences Union* **6**, 1 pp., Available as http://www.cosis.net/abstracts/EGU04/04896/EGU04-J-04896.

Müller, M. D. and Scherer, D. 2005. A grid- and subgrid-scale radiation parametrization of topographic effects for mesoscale weather forecast models. *Mon. Wea. Rev.* **133**, 1431–1442.

Niemelä, S., Räisänen, P. and Savijärvi, H. 2001a. Comparison of surface radiative flux parametrizations. Part I: longwave radiation. *Atmosph. Res.* **58**, 1–18.

Niemelä, S., Räisänen, P. and Savijärvi, H. 2001b. Comparison of surface radiative flux parametrizations. Part II: shortwave radiation. *Atmosph. Res.* **58**, 141–154.

Nunes, M., Elliason, I. and Lindgren, J. 2000. Spatial variation of incoming longwave radiation in Göteborg, Sweden. *Theor. Appl. Climatol.* **67**, 181–192.

Oliphant, A. J., Spronken-Smith, R. A., Sturman, A. P. and Owens, I. F. 2003. Spatial variability of surface radiation fluxes in mountainous terrain. *J. Appl. Meteor.* **42**, 113–128.

Paltridge, G. and Platt, C. M. R. 1976. *Radiative Processes in Meteorology and Climatology*. Elsevier Scientific Publishing company, New York, 318 pp.

Räisänen, P., Rummukainen, M. and Räisänen, J. 2000. Modification of the Hirlam radiation scheme for use in the Rossby Centre regional atmospheric climate model. Technical Report 49, Department of Meteorology, University of Helsinki, 71. Available at http://www.meteo.helsinki.fi.

Rodriguez, E., Navascués, B., Ayuso, J. J. and Järvenoja, S. 2003. Analysis of surface variables and parameterization of surface processes in HIRLAM. Part I: approach and verification by parallel runs. Technical report, HIRLAM, 52 pp. Available at http://hirlam.knmi.nl.

Rontu, L., 2006. A study on parametrization of orography-related momentum fluxes in a synoptic-scale NWP model. *Tellus* **58A**, 68–81.

Savijärvi, H. 1990. Fast radiation parameterization schemes for mesoscale and short-range forecast models. *J. Appl. Meteor.* **29**, 437–447.

Savijärvi, H., Arola, A. and Räisänen, P. 1997. Shortwave optical properties of precipitating waterclouds. *Quart. J. Roy. Met. Soc.* **123**, 883–899.

USGS, 1998. GTOPO30, Global 30 Arc Second Elevation data set. U.S. Geological Survey, available at http://edcdaac.usgs.gov/gtopo30/gtopo30.html.

USGS, 2003. Hydro1k elevation derivative database. http://edcdaac.usgs.gov/gtopo30/hydro/readme.html.

van Meijgaard, E., Andrae, U. and Rockel, B. 2001. Comparison of model predicted cloud parameters and surface radiation fluxes with observations in the 100 km scale. *Meteor. Atmos. Phys.* **77**, 109–120.

Whiteman, C. D., Allwine, K. J., Fritschen, L. J., Orgill, M. M. and Simpson, J. R. 1989a. Deep valley radiation and surface energy budget microclimates. Part I: radiation. *J. Appl. Meteor.* **28**, 414–426.

Whiteman, C. D., Allwine, K. J., Fritschen, L. J., Orgill, M. M. and Simpson, J. R. 1989b. Deep valley radiation and surface energy budget microclimates. Part II: energy budget. *J. Appl. Meteor.* **28**, 427–437.

Wyser, K., Rontu, L. and Savijärvi, H. 1999. Introducing the effective radius into a fast radiation scheme of a mesoscale model. *Contr. Atm. Phys.* **72**, 205–218.